

***L*-shell ionization of intermediate- and high-*Z* elements by alpha particles\***T. L. Hardt<sup>†</sup> and R. L. Watson*Department of Chemistry and Cyclotron Institute, Texas A&M University, College Station, Texas 77843*

(Received 12 February 1976)

*L* x-ray production cross sections have been measured for thin targets of Sn, Te, Nd, Tb, Tm, Au, and Pb using 30- to 80-MeV alpha particles. Theoretical atomic parameters were used to deduce *L*-subshell ionization cross sections for Tb, Tm, Au, and Pb, and average *L*-shell fluorescence yields were used to obtain total *L*-shell ionization cross sections for Sn, Te, and Nd. The experimental results are compared with previous proton and alpha-particle measurements, and with the predictions of plane-wave Born, semiclassical, and binary-encounter approximation treatments of *L*-shell ionization. Generally good agreement with the PWBA calculations is found for these relatively high-energy measurements, although several systematic discrepancies are observed.

## I. INTRODUCTION

In recent years, extensive experimentation dealing with x-ray production by protons and  $\alpha$  particles has been carried out. Experimental x-ray yield measurements have provided information relating to the cross sections for creating inner-shell vacancies and high-resolution spectral measurements have given information pertaining to the states of excitation produced in the collisions.<sup>1,2</sup>

Aside from the fundamental utility of x-ray production measurements for the characterization of ionizing atomic collisions, they have also proven to be of practical applicability for trace-element analyses of biological and environmental samples.<sup>3</sup> Additionally, x-ray yields may be used to accurately determine beam intensities in various other particle-accelerator experiments.

A comprehensive collection of cross sections for *K*-shell ionization by light ions incident on a wide variety of targets over a large range of projectile energies has accumulated in the literature.<sup>4</sup> Measurements of *L* x-ray production cross sections have thus far been more restricted both in target atomic number and in projectile energy.<sup>5</sup> Very few measurements have been performed at particle energies above 5 MeV/amu.

The present work has been directed toward extending the body of data on *L*-shell ionization to higher projectile energies. We report here on measurements of *L* x-ray yields for targets of Sn, Te, Nd, Tb, Tm, Au, and Pb produced by  $\alpha$  particles ranging in energy from 7.5 to 20 MeV/amu. Total *L*-shell ionization cross sections were deduced from the data for all of the above-mentioned targets and *L*-subshell ionization cross sections were obtained for Tb, Tm, Au, and Pb.

## II. EXPERIMENTAL METHODS

The yield of x rays from each target of interest was measured simultaneously with the x-ray yield

of a reference element by irradiating a target stack composed of both elements. Each target stack was made by evaporating (under high vacuum) the reference element onto a thin Mylar backing ( $\sim 520 \mu\text{g}/\text{cm}^2$ ) and then evaporating the target element on top of the reference element. The target ele-

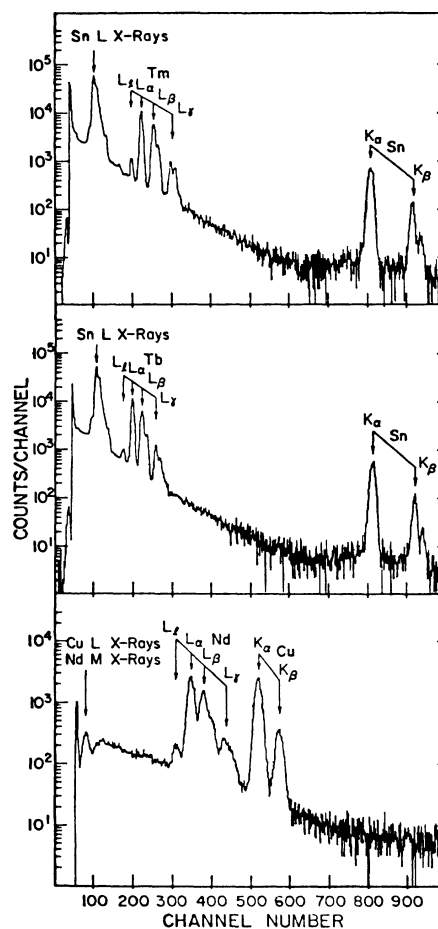


FIG. 1. Sample x-ray spectra obtained for Tm, Tb, and Nd target stacks with 30-MeV  $\alpha$  particles.

ment effective thickness (corrected for the  $45^\circ$  inclination angle) ranged from 67 to  $188 \mu\text{g}/\text{cm}^2$  and in all cases the target-plus-reference thickness was sufficiently thin that projectile energy loss could be neglected. In this way, the  $L$  x-ray yields of Sn, Tb, Tm, Au, and Pb were measured relative to the  $K$  x-ray yield of Sn, and the  $L$  x-ray yields of Te and Nd were measured relative to the  $K$  x-ray yields of Te and Cu, respectively.

All of the measurements were performed with a Si(Li) detector system (250 eV full width at half-maximum at 6.4 keV) located a distance of 18.4 cm from the target. The detector was positioned at  $90^\circ$  with respect to the beam and was separated from the target by a  $3.3\text{-mg}/\text{cm}^2$  Be window (which was part of the detector cryostat). Sample spectra for Tm, Tb, and Nd target stacks obtained with 30-MeV  $\alpha$  particles are shown in Fig. 1.

The efficiency calibration procedure was the same as that described in Ref. 6. It was extended down to 3.25 keV by measuring the ratio of Np  $M$  to  $L\alpha$  x-rays emitted by a thin  $^{241}\text{Am}$  source. The absolute intensity ratio of these two peaks has been found to be  $0.470 \pm 0.045$  by Karttunen *et al.*<sup>7</sup> Further details of the experimental procedures are given in Refs. 6 and 8.

### III. DATA ANALYSIS AND RESULTS

Relative x-ray yields were determined from the integrated  $L$  x-ray photopeaks of the elements of interest and the integrated  $K\alpha$  x-ray photopeaks of the reference elements. For the elements Tb, Tm, Au, and Pb, where the various major  $L$  x-ray groups were sufficiently resolved, individual group ( $Ll$ ,  $L\alpha$ ,  $L\beta$ , and  $L\gamma$ ) photopeak intensities were obtained by least-squares fitting. The photopeak intensity ratios were then corrected for detector efficiency and absorption (see Ref. 6). Using the absolute "smoothed"  $K$  x-ray production cross sections reported previously<sup>6</sup> for the reference elements, absolute  $L$  x-ray production cross sections were determined. A more refined set of x-ray production cross sections was obtained by plotting the experimental values as a function of atomic number at each  $\alpha$ -particle energy. Smooth curves were then fitted through the data sets and "smoothed"  $L$  x-ray production cross sections were read from them. The values of the "smoothed"  $L$  x-ray production cross sections are listed in Table I. The errors associated with these values are estimated to be  $\pm 10\%$  on the average.

The conversion of  $L$  x-ray production cross sections to ionization cross sections is complicated because (i) three subshells contribute to the total cross section, and (ii) vacancies created

TABLE I. "Smoothed"  $L$  x-ray production cross sections (in b) for ionization by  $\alpha$  particles.

Energy (MeV)	$\sigma_L^*$ (b)						
	$_{50}\text{Sn}$	$_{52}\text{Te}$	$_{60}\text{Nd}$	$_{65}\text{Tb}$	$_{69}\text{Tm}$	$_{79}\text{Au}$	$_{82}\text{Pb}$
30	5050	4770	3550	2790	2180	1075	845
40	5610	5460	4580	3800	3170	1575	1300
50	5710	5600	4870	4200	3560	2050	1650
60	5650	5550	4900	4300	3750	2410	2060
70	5570	5510	5190	4700	4170	2520	2130
80	5130	5220	5080	4620	4150	2710	2300

in the lower two  $L$  subshells ( $2s$  and  $2p_{1/2}$ ) can be shifted to higher subshells ( $2p_{1/2}$  and  $2p_{3/2}$ ) via Coster-Kronig transitions. Hence the total  $L$  x-ray production cross section  $\sigma_L^*$  cannot be related directly to the total  $L$ -shell ionization cross section, but must rather be expressed as a sum of subshell ionization cross sections  $\sigma_{Li}$  such that

$$\sigma_L^* = \sum_{i=1}^3 \nu_{Li} \sigma_{Li}, \quad (1)$$

where the  $\nu_{Li}$  are  $L$ -subshell fluorescence yields corrected for vacancy transfer. Since many of the transitions to each subshell are so closely spaced in energy that they are not fully resolvable, and because very few experimental data are available on subshell fluorescence yields, it is not presently possible to determine  $L$ -subshell ionization cross sections directly. Nevertheless, a number of previous workers have devised methods with which  $L$ -subshell ionization cross sections may be deduced by using theoretical values of partial radiative widths and  $L$ -subshell fluorescence and Coster-Kronig yields.<sup>9-11</sup> In the present work, we have deduced  $L$ -subshell ionization cross sections using a procedure (described in detail by Chang *et al.*<sup>12</sup>) which involves an analysis of the  $L\alpha$  photopeak and the various components of the  $L\gamma$  photopeak.

Using a least-squares peak-resolving program, the  $L\gamma$  photopeaks of Tb, Tm, Au, and Pb were resolved into four Gaussian components representing the  $L\gamma_5$ ,  $L\gamma_1$ ,  $L\gamma_{2+3+6}$ , and  $L\gamma_4$  x-ray lines. One of the fitted spectra for 40-MeV  $\alpha$  particles incident on Pb is shown in Fig. 2. Also shown in this figure is a spectrum obtained with protons of the same velocity (10 MeV) incident on the same target.

The  $L_1$ -subshell ionization cross sections were determined using the expression

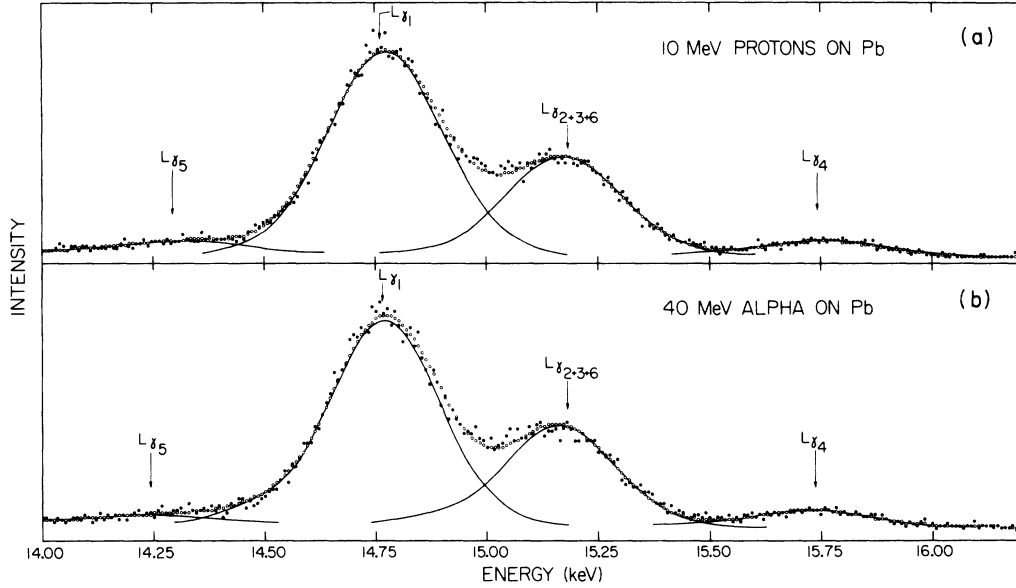


FIG. 2. Least-squares analysis of the  $L\gamma$  x-ray groups of Pb resulting from bombardment with (a) 10-MeV protons and (b) 40-MeV  $\alpha$  particles.

$$\sigma_{L_1} = \frac{\sigma_{L\gamma_{5+1}}^* (\omega_2 F_{2\gamma}) - \sigma_{L\gamma}^* (\omega_2 F_{2\gamma_{5+1}})}{(\omega_2 F_{2\gamma}) (f_{12} \omega_2 F_{2\gamma_{5+1}}) - (\omega_1 F_{1\gamma} + f_{12} \omega_2 F_{2\gamma}) (\omega_2 F_{2\gamma_{5+1}})}, \quad (2)$$

which was obtained by solving Eqs. (1d) and (3) in Ref. 12 simultaneously. The  $L_2$ -subshell ionization cross sections were then determined using the expression

$$\sigma_{L_2} = \frac{\sigma_{L\gamma}^* - \sigma_{L_1} (\omega_1 F_{1\gamma} + f_{12} \omega_2 F_{2\gamma})}{\omega_2 F_{2\gamma}}, \quad (3)$$

which was obtained from Eq. (1d) of Ref. 12, and the  $L_3$ -subshell ionization cross sections were finally determined using the expression

$$\sigma_{L_3} = \frac{\sigma_{L\alpha}^* - [\sigma_{L_1} (f_{13} + f_{12} f_{23}) + \sigma_{L_2} f_{23}] \omega_3 F_{3\alpha}}{\omega_3 F_{3\alpha}}, \quad (4)$$

which was obtained from Eq. (1b) of Ref. 12. In all of the above expressions, the  $\omega_i$  are subshell fluorescence yields, the  $f_{ij}$  are Coster-Kronig yields, and the  $F_{ij}$  are the various partial radiative widths (i.e.,  $F_{3\alpha} = \Gamma_{L_3\alpha} / \Gamma_{L_3}$ ). The values of the  $L$ -subshell fluorescence yields and the Coster-Kronig yields used in the present work were taken from the theoretical results of McGuire<sup>13</sup> and the partial radiative widths were obtained from the theoretical results of Scofield.<sup>14</sup> For convenient reference, they are listed in Table II.

The use of atomic parameters calculated for single-vacancy states in the above analysis procedure assumes that multiple ionization is relatively im-

TABLE II. Theoretical  $L$ -subshell fluorescence yields, Coster-Kronig yields, and partial widths used in this work.

Target	$L$ -subshell fluorescence yields <sup>a</sup>			$L$ -subshell Coster-Kronig yields <sup>a</sup>			Partial radiative widths <sup>b</sup>						
	$\omega_1$	$\omega_2$	$\omega_3$	$f_{12}$	$f_{13}$	$f_{23}$	$F_{1\gamma}$	$F_{2\gamma}$	$F_{2\gamma_{5+1}}$	$F_{1\beta}$	$F_{2\beta}$	$F_{3\beta}$	$F_{3\alpha}$
<sup>85</sup> Tb	0.101	0.180	0.178	0.203	0.307	0.139	0.207	0.150	0.149	0.777	0.828	0.147	0.819
<sup>69</sup> Tm	0.113	0.225	0.216	0.199	0.316	0.134	0.211	0.152	0.153	0.774	0.826	0.147	0.814
<sup>79</sup> Au	0.105	0.357	0.327	0.083	0.644	0.132	0.222	0.179	0.163	0.747	0.799	0.172	0.787
<sup>82</sup> Pb	0.116	0.403	0.373	0.073	0.652	0.109	0.227	0.188	0.167	0.735	0.789	0.180	0.777

<sup>a</sup> From Reference 13.

<sup>b</sup> From Reference 14.

TABLE III.  $L$ -subshell ionization cross sections for ionization by  $\alpha$  particles (in units of  $10^3$  b).

Energy (MeV)	$^{65}\text{Tb}$			$^{69}\text{Tm}$			$^{79}\text{Au}$			$^{82}\text{Pb}$		
	$L_1$	$L_2$	$L_3$									
30	4.24	3.26	7.22	2.51	2.22	4.78	0.874	0.638	1.57	0.764	0.409	0.976
40	5.38	5.47	9.10	3.54	3.26	7.05	1.32	0.855	2.36	0.821	0.705	1.78
50	5.83	5.34	11.0	3.69	3.56	8.33	1.74	1.20	2.94	0.984	0.876	2.35
60	5.89	5.29	11.5	4.38	3.72	8.29	1.95	1.45	3.51	1.31	1.13	2.80
70	7.26	5.14	12.9	4.25	4.55	9.39	2.11	1.65	3.43	1.59	1.16	2.65
80	6.43	4.89	12.5	4.44	4.36	9.31	2.15	1.74	3.85	1.82	1.26	2.76

probable. From the high-resolution measurements of Olsen *et al.*<sup>15</sup> for Sn, we estimate that simultaneous  $M$ -shell vacancies are created in roughly 4% of the  $L$ -shell ionizing collisions at the lowest energy used in the present study. It is expected that the degree of simultaneous  $M$ -shell ionization will decrease with increasing projectile energy and target atomic number.

The  $L$ -shell ionization cross sections for Tb, Tm, Au, and Pb are listed in Table III. A self-consistency check of these subshell ionization cross sections was made by using them to predict the  $L\beta$  x-ray production cross sections. Overall agreement to within  $\pm 5\%$  was obtained between the predicted and the measured  $L\beta$  x-ray cross sections. However, because of the uncertainties involved in the use of the theoretical atomic parameters, the absolute  $L$ -subshell cross sections may be in error by as much as  $\approx 30\%$ .

Because the resolution of the  $L$  x-ray lines in the Sn, Te, and Nd spectra was not sufficient to extract subshell cross sections by the method discussed above, ionization cross sections could not be obtained directly from the data without the use of average  $L$ -shell fluorescence yields. The experimental  $L$ -shell fluorescence yields  $\bar{\omega}_L$  tabulated by Bambynek *et al.*<sup>16</sup> show a large uncertainty over the range of atomic numbers used in this study. Moreover, these fluorescence-yield measurements were made for ionization by photons and electrons and hence may reflect quite different initial subshell vacancy distributions than are formed in ionization by heavy-charged-particle bombardment. However, having deduced the  $L$ -shell ionization cross sections for Tb, Tm, Au, and Pb, it was possible to evaluate their average  $L$ -shell fluorescence yields from the relationship

$$\bar{\omega}_L = \sigma_L^* / \sigma_L. \quad (5)$$

The values so obtained are compared in Fig. 3 with various experimental values tabulated in Ref. 16. As can be seen, the deduced fluorescence yields define a straight line which coincides, on the average, with the results obtained using photons or electrons. This indicates that the initial subshell vacancy distributions created in high-energy  $\alpha$ -particle bombardment are indeed similar to those for photon fluorescence and electron bombardment. The curve can be extended down to  $Z=50$ , where the previous data become sparse and begin to deviate wildly. Assuming a linear extrapolation, the values of  $\bar{\omega}_L$  obtained for Sn, Te, and Nd were 0.096, 0.105, and 0.150, respectively. Using these extrapolated  $\bar{\omega}_L$  values, total  $L$ -shell ionization cross sections were then calculated from the  $L$  x-ray production cross sections listed in Table I.

#### IV. DISCUSSION

In Fig. 4(a) the experimental  $L$ -shell ionization cross sections for Tm are compared with the results of plane-wave-Born-approximation<sup>17,18</sup> (PWBA), semiclassical-approximation<sup>19,20</sup> (SCA),

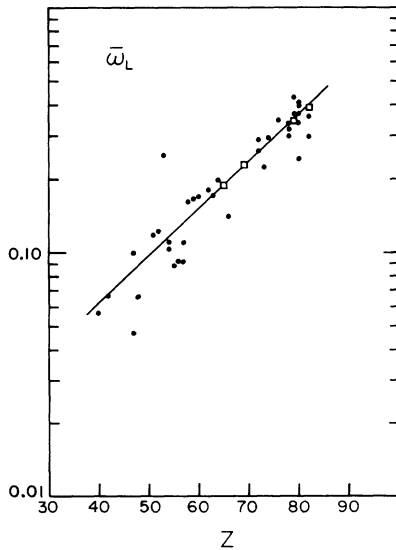


FIG. 3. Comparison of the average  $L$ -shell fluorescence yields of Tb, Tm, Au, and Pb deduced from the present measurements (open squares) with data tabulated in Ref. 16 (solid circles).

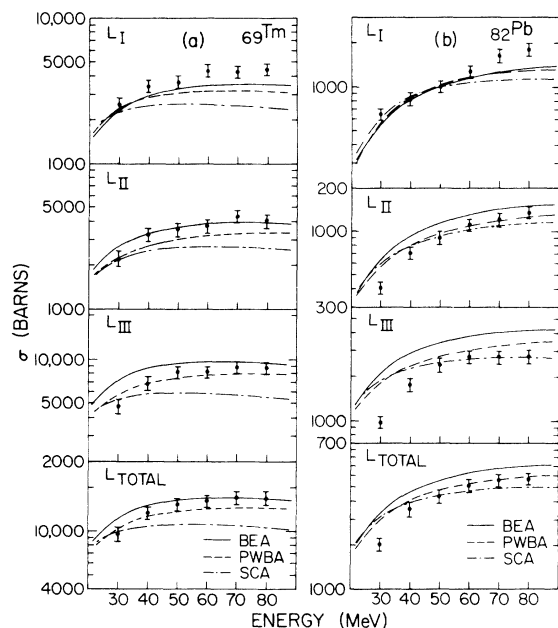


FIG. 4. (a) Comparison of the  $L$ -subshell ionization cross sections for Tm with the predictions of the BEA, PWBA, and SCA theories. (b) Same as (a), but for Pb.

and binary-encounter-approximation<sup>21</sup> (BEA) calculations. (The error bars represent the relative uncertainties only.) It is observed that the  $L_1$ -subshell cross sections are somewhat higher ( $\sim 15$ – $20\%$ ) than the BEA and PWBA predictions, whereas the  $L_2$ - and  $L_3$ -subshell ionization cross sections generally lie between the BEA and PWBA results. Overall, the total  $L$ -shell ionization cross sections are represented about equally well by both the BEA and the PWBA. The SCA results, on the other hand, are consistently lower ( $\sim 30\%$ ) than the experimental cross sections, except at the lowest energies. Essentially the same trends were also observed in a similar comparison made with the Tb data.<sup>8</sup>

The experimental  $L$ -subshell ionization cross sections for Pb are compared with the various theoretical predictions in Fig. 4(b). (The error bars represent the relative uncertainties only.) Here it is observed that the  $L_1$ -subshell cross sections are in good agreement with all three theories at the low-energy end of the excitation function but that they rise above the various theoretical results at the higher  $\alpha$ -particle energies. The  $L_2$ - and  $L_3$ -subshell cross sections are in good agreement with the PWBA and SCA results at energies above 50 MeV, but drop considerably below the predictions of both of these theories at the low-energy end of the excitation function. Overall, the BEA predictions are  $\sim 30\%$  higher than the experimental results for the  $L_2$  and  $L_3$  subshells. Essentially the

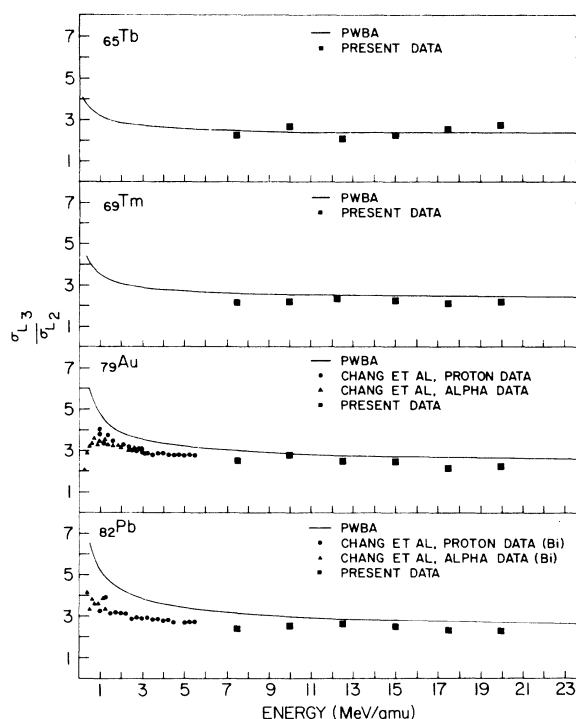


FIG. 5. Comparison of the ionization cross section ratios  $\sigma_{L_3}/\sigma_{L_2}$  for Tb, Tm, Au, and Pb with the data of Chang *et al.* (Ref. 12) and the PWBA predictions.

same trends were also observed in a similar comparison made with the Au data.<sup>8</sup>

Because of the uncertainties associated with the use of theoretical values of the various atomic parameters in the data analysis, a detailed discussion of absolute-cross-section differences of less than  $\sim 30\%$  between theory and experiment would not be particularly meaningful. However, a more stringent comparison can be made using cross-section ratios in which, as has been pointed out by numerous other authors,<sup>9–12</sup> many of the uncertainties cancel. In Fig. 5 is presented a comparison of the experimental  $L_3$ - to  $L_2$ -subshell ionization cross-section ratios for Tb, Tm, Au, and Pb with those predicted by the PWBA. Also shown in this figure are the data of Chang *et al.*<sup>12</sup> for protons and  $\alpha$  particles on Au and Bi. It is seen that at low energies (data of Chang *et al.*) the ratios are considerably below the PWBA curves, but at the higher energies the data agree much better with the theoretical predictions. These results confirm the expectation that the PWBA should more accurately describe ionization by high-energy projectiles for which the conditions of validity of the PWBA are better fulfilled.

The total  $L$ -shell ionization cross sections obtained in the present study are compared with the results obtained with protons and  $\alpha$  particles by

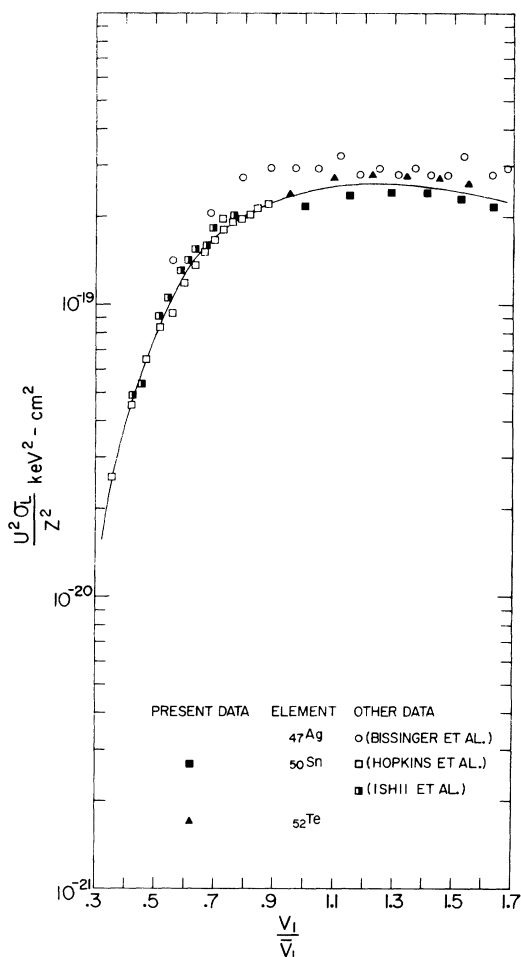


FIG. 6. Total  $L$ -shell ionization cross sections for  $Z = 47-52$  including data from Refs. 22-24.

other experimenters in Figs. 6-10. In these figures all previous data have been converted from x-ray cross sections to ionization cross sections using average  $L$ -shell fluorescence yields read from the straight line in Fig. 3. The ionization cross sections have been multiplied by the factor  $u^2/z^2$ , where  $u$  is the weighted-average  $L$ -shell binding energy and  $z$  is the projectile atomic number, and are plotted as a function of the velocity ratio

$$\frac{v_1}{v_L} = \left( \frac{m E}{u M} \right)^{1/2},$$

where  $m$  is the electron mass,  $E$  is the projectile energy, and  $M$  is the projectile mass. Included in these figures are the recent  $L$ -shell cross section data for Ag (Bissinger *et al.*<sup>22</sup>), Sn (Hopkins *et al.*<sup>23</sup>), Sn and Ta (Ishii *et al.*<sup>24</sup>), Pr, Sm, and Dy (Abrath and Gray<sup>25</sup>), Gd, Lu, and Au (Flochinn<sup>26</sup>), Au (Shafroth *et al.*<sup>27</sup>), Pb (Busch *et al.*,<sup>28</sup>

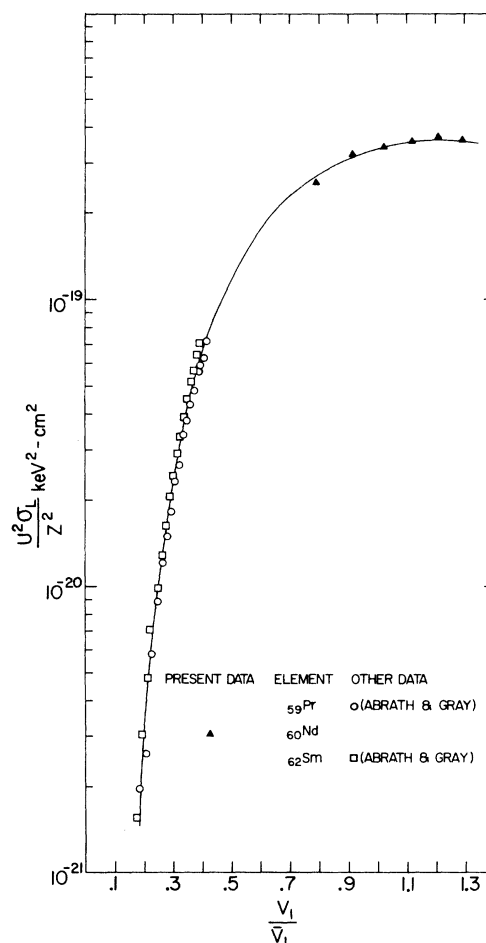


FIG. 7. Total  $L$ -shell ionization cross sections for  $Z = 59-62$ , including data from Ref. 25.

Tawara *et al.*<sup>29</sup>), and Ta, Au, and Bi (Chang *et al.*<sup>12</sup>).

Fairly good agreement is found between the previous measurements and the results of the present work. Together, the various sets of data define the  $L$ -shell excitation function over almost three orders of magnitude. Smooth curves have been drawn through an average of the combined data for each group of atomic numbers and these "average" curves are compared in Fig. 11 with the BEA and PWBA predictions. (The PWBA results for the region bounded by Sn at the bottom and Au at the top are shown by the crosshatched area.) It can be seen that at very low velocity ratios, the experimental data for  $Z = 59-66$  and  $Z = 69-83$  fall above the BEA and PWBA by nearly an order of magnitude. The addition of binding and Coulomb corrections to the PWBA<sup>30</sup> would lower the predicted cross sections and thereby make the agreement with the experimental data even worse. As the velocity ratio increases, the experimental

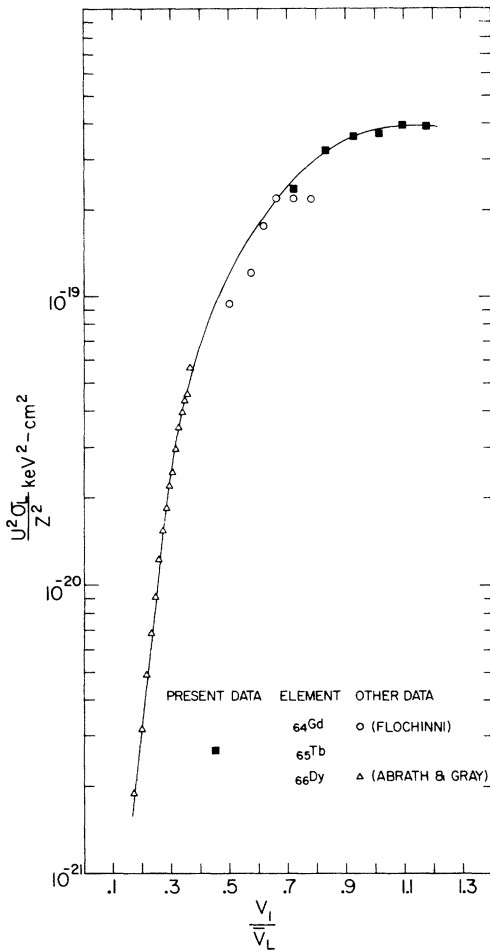


FIG. 8. Total  $L$ -shell ionization cross sections for  $Z = 64-66$ , including data from Refs. 26 and 25.

curves cross through the theoretical curves and then diverge from one another as they approach their maxima. The PWBA calculations predict the occurrence of maxima in the excitation functions for  $Z = 50, 60,$  and  $65$  at velocity ratios of 1.13, 1.11, and 1.10, respectively, whereas the BEA results predict a common maximum for all atomic numbers at a velocity ratio of 1.00. Although the experimental curves display maxima which shift to lower velocity ratios with increasing atomic number, in accordance with the PWBA results, they are spread much farther apart than predicted. The experimental maxima are located at approximate velocity ratios of 1.3, 1.2, and 1.1 for  $Z = 50, 60,$  and  $65$ , respectively.

Another feature of the experimental excitation functions in the region near their maxima is that they increase relative to one another in going from the  $Z = 47-52$  curve to the  $Z = 64-66$  curve, but then the ordering reverses and they decrease relative to one another in going from the  $Z = 64-66$

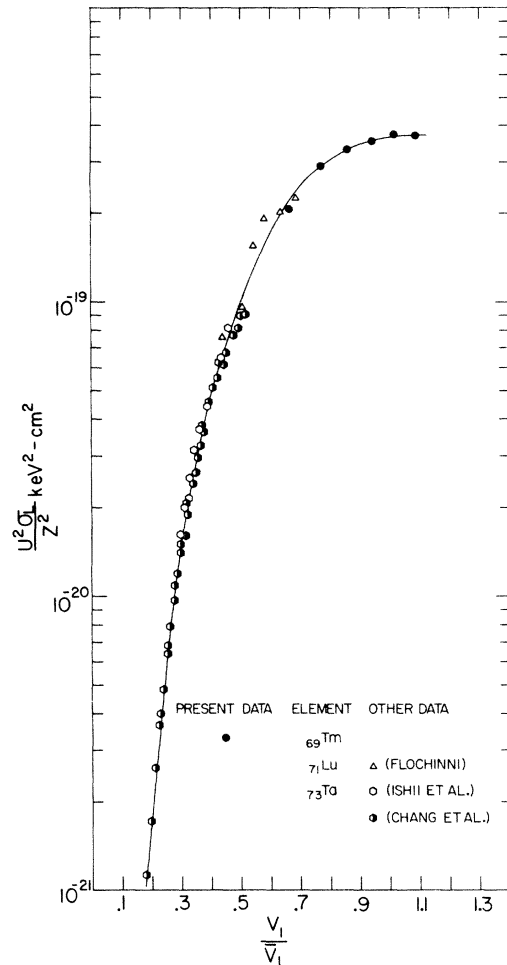


FIG. 9. Total  $L$ -shell ionization cross sections for  $Z = 69-73$ , including data from Refs. 26, 24, and 12.

curve to the  $Z = 79-83$  curve. The PWBA calculations (as shown by the crosshatched area in Fig. 11) predict steadily increasing excitation functions with increasing  $Z$ .

## V. CONCLUSIONS

The present investigations have focused on the high-energy region of the excitation functions for  $L$ -shell ionization of intermediate to heavy atoms by  $\alpha$  particles. In this energy region the conditions for the applicability of the PWBA, SCA, and BEA are reasonably well satisfied, and projectile binding and deflection effects are negligibly small. It has been found from the data obtained in this study, in combination with the data of others, that for  $v_1/\bar{v}_L \geq 0.7$  the PWBA description reproduces the experimental cross sections to better than 30% over a range of atomic numbers extending from

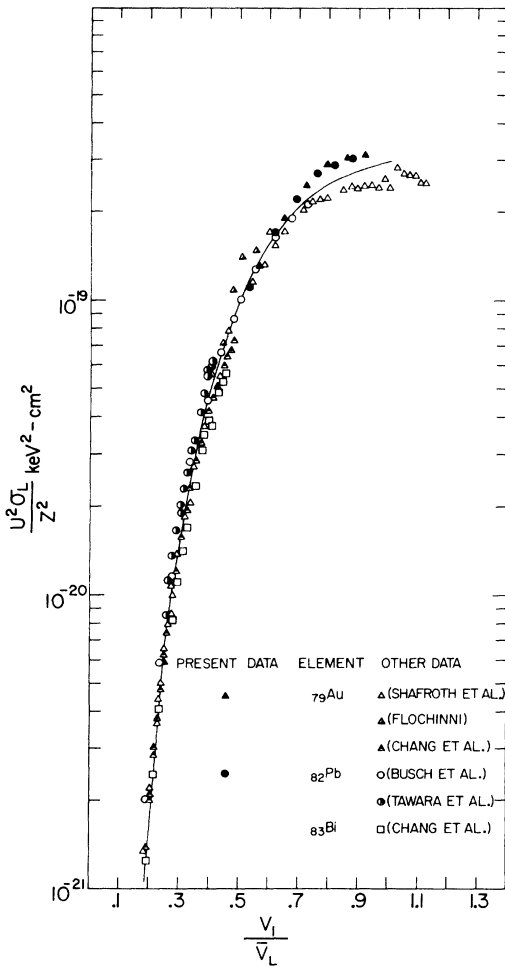


FIG. 10. Total *L*-shell ionization cross sections for *Z* = 79–83, including data from Refs. 12 and 26–29.

*Z* = 50 to *Z* = 83, while the BEA gives cross sections which are generally somewhat less accurate. Below  $v_1/\bar{v}_L = 0.3$  differences between both theories and experiment become as large as an order of magnitude.

Despite the fairly good agreement displayed between the PWBA and the experimental results in the high-energy region, certain details of the data do not appear to be consistent with the theoretical predictions. In particular, the positions of the maxima in the experimental excitation functions for *Z* = 47–62 occur at higher velocity ratios than predicted. Additionally, the apparent reversal in the ordering of the excitation functions with decreasing atomic number is contrary to the pre-

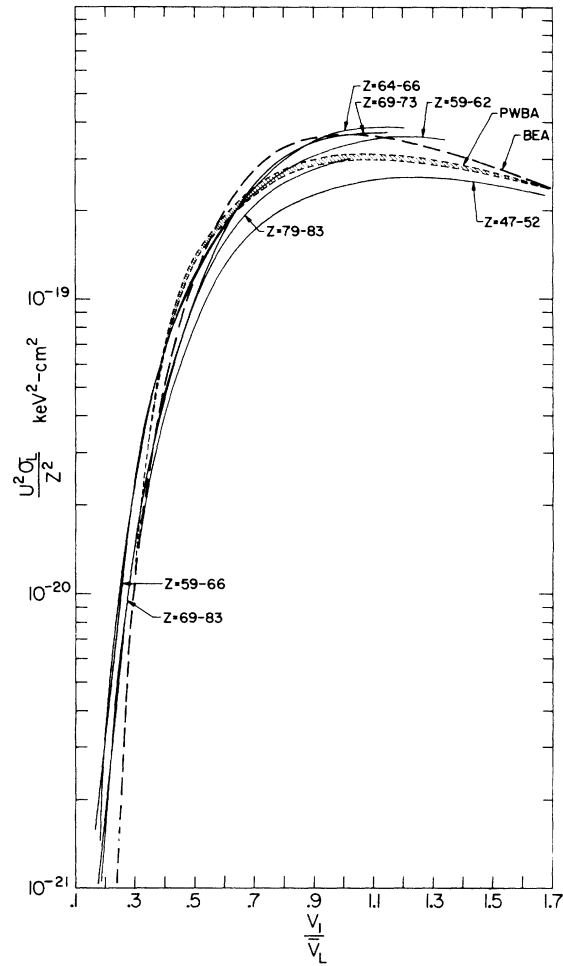


FIG. 11. Comparison of the “average” *L*-shell ionization cross-section curves with the predictions of the BEA and PWBA. (The PWBA results for the region bounded by *Z* = 50 and *Z* = 79 is shown by the cross-hatched area.)

dicted trend. This feature however may simply be a consequence of the linear extrapolation used in obtaining the average *L*-shell fluorescence yields for converting the x-ray cross sections to ionization cross sections.

ACKNOWLEDGMENTS

We thank Joaquin Hernandez for making the evaporated targets used in this work. The assistance of the operations personnel (particularly W. Walterscheid) of the Cyclotron Institute of Texas A&M University is gratefully acknowledged.

- \*Supported in part by the U. S. Energy Research and Development Administration and the Robert A. Welch Foundation.
- † Present address: Dept. of Chemical and Nuclear Engineering, Washington State Univ., Pullman, Wash. 99163.
- <sup>1</sup>J. D. Garcia, R. J. Fortner, and T. M. Kavanagh, *Rev. Mod. Phys.* 45, 111 (1973).
- <sup>2</sup>Patrick Richard, in *Atomic Inner-Shell Processes*, edited by B. Crasemann (Academic, New York, 1975), Vol. I, p. 74.
- <sup>3</sup>See, for example, F. Folkmann, C. Gaarde, T. Huus, and K. Kemp, *Nucl. Instrum. Methods* 116, 487 (1974).
- <sup>4</sup>See the references given by C. H. Rutledge and R. L. Watson, *At. Data Nucl. Data Tables* 12, 195 (1973).
- <sup>5</sup>See the references given by T. L. Hardt and R. L. Watson, *At. Data Nucl. Data Tables* (to be published).
- <sup>6</sup>T. L. Hardt and R. L. Watson, *Phys. Rev. A* 7, 1917 (1973).
- <sup>7</sup>E. Karttunen, H. U. Freund, and R. W. Fink, *Phys. Rev. A* 4, 1695 (1971).
- <sup>8</sup>T. L. Hardt, Ph.D. thesis (Texas A & M University, 1975) (unpublished).
- <sup>9</sup>D. H. Madison, A. B. Baskin, C. E. Busch, and S. M. Shafroth, *Phys. Rev. A* 9, 675 (1974).
- <sup>10</sup>S. Datz, J. L. Duggan, L. C. Feldman, E. Laegsgaard, and J. U. Anderson, *Phys. Rev. A* 9, 192 (1973).
- <sup>11</sup>F. Abrath and T. J. Gray, *Phys. Rev. A* 9, 682 (1974).
- <sup>12</sup>C. N. Chang, J. F. Morgan, and S. L. Blatt, *Phys. Rev. A* 11, 607 (1975).
- <sup>13</sup>E. J. McGuire, *Phys. Rev. A* 3, 587 (1971).
- <sup>14</sup>J. H. Scofield, *Phys. Rev.* 179, 9 (1969).
- <sup>15</sup>D. K. Olsen, C. F. Moore, and P. Richard, *Phys. Rev. A* 7, 1244 (1973).
- <sup>16</sup>W. Bambynek, B. Crasemann, R. W. Fink, H. U. Freund, H. Mark, C. D. Swift, R. E. Price, and P. V. Rao, *Rev. Mod. Phys.* 44, 716 (1972).
- <sup>17</sup>G. S. Khandelwal, B. H. Choi, and E. Merzbacher, *At. Data* 1, 103 (1969).
- <sup>18</sup>B. H. Choi, E. Merzbacher, and G. S. Khandelwal, *At. Data* 5, 291 (1973).
- <sup>19</sup>J. M. Hansteen and O. P. Mosebekk, *Nucl. Phys. A* 201, 541 (1973).
- <sup>20</sup>L. Kocback, Dept. of Physics, Univ. of Bergen, Bergen, Norway, Report No. 58, 1973 (unpublished).
- <sup>21</sup>J. S. Hansen, *Phys. Rev. A* 8, 822 (1973).
- <sup>22</sup>G. A. Bissinger, S. M. Shafroth, and A. W. Waltner, *Phys. Rev. A* 5, 2046 (1972).
- <sup>23</sup>F. Hopkins, R. Brenn, A. R. Whitemore, J. Karp, and S. K. Bhattacharjee, *Phys. Rev. A* 11, 916 (1975).
- <sup>24</sup>K. Ishii, S. Morita, H. Tawara, H. Kaji, and T. Shiokawa, *Phys. Rev. A* 11, 119 (1975).
- <sup>25</sup>F. Abrath and T. J. Gray, *Phys. Rev. A* 10, 1157 (1974).
- <sup>26</sup>R. G. Flocchini, Ph.D. thesis (Univ. of California at Davis, 1974) (unpublished).
- <sup>27</sup>S. M. Shafroth, G. A. Bissinger, and A. W. Waltner, *Phys. Rev. A* 7, 566 (1973).
- <sup>28</sup>C. E. Busch, A. B. Baskin, P. H. Nettles, and S. M. Shafroth, *Phys. Rev. A* 7, 1601 (1973).
- <sup>29</sup>H. Tawara, K. Ishii, S. Morita, H. Kaji, C. N. Hsu, and T. Shiokawa, *Phys. Rev. A* 9, 1617 (1974).
- <sup>30</sup>W. Brandt and G. Lapicki, *Phys. Rev. A* 10, 474 (1974).